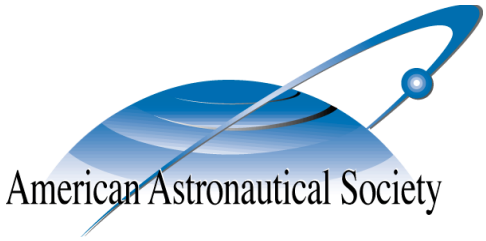

Orbit-Nadir Aligned Coulomb Tether Reconfiguration Analysis

Arun Natarajan and Hanspeter Schaub

Simulated Reprint from

Journal of the Astronautical Sciences
Vol. 56, No. 4, Oct.–Dec., 2008, Pages 573–592

A publication of the
American Astronautical Society
AAS Publications Office
P.O. Box 28130
San Diego, CA 92198

Journal of the Astronautical Sciences, Vol. 56, No. 4, Oct.–Dec., 2008, Pages 573–592

Orbit-Nadir Aligned Coulomb Tether Reconfiguration Analysis

Arun Natarajan* **and Hanspeter Schaub†**

Abstract

The reconfiguring of a two craft Coulomb tether, aligned along the orbit radial direction, is studied. The linearized out-of-plane equation of motion is decoupled and not influenced by Coulomb forces. Previous research assumes this out-of-plane motion is controlled with conventional thrusting to keep it within a specified bound. An analytical solution is developed for the linearized charged out-of-plane relative motion using Bessel functions for the special reconfiguration case where the prescribed expansion or contraction rate is constant. Bounds on the initial out-of-plane oscillation are deduced such that the final oscillation will remain within the prescribed limits. These analytical results assist Coulomb tether reconfiguration maneuvers in determining when conventional thrusting must be employed to damp out-of-plane motion. Further, an improved reconfiguration strategy is analyzed where the on/off switches of the constant rate reconfiguration expansion are smoothed to reduce transient oscillations. This modification is shown to have minimal impact on the predicted out-of-plane motion.

Introduction

Formation flying of spacecraft using Coulomb forces is a new and emerging field of study. The electrostatic (Coulomb) charge of the spacecraft is varied by active emission of either negative electric charges (electrons) or positive electric charges (ions). The resulting changes in inter-spacecraft Coulomb forces are used to control the relative motion of the spacecraft. Due to the drop off of the electrostatic force with distance, close proximity flying missions are considered with separation distances ranging up to 100 meters. Coulomb thrusting requires essentially no consumables (fuel efficiencies ranging up to 10^{13} seconds), requires very little electric power to operate (often less than 1 Watt), and can be controlled with a high bandwidth (zero to maximum charge transition times are of the order of milli-seconds).[1] Also, by using this method the thruster exhaust plume contamination issues with neighbouring satellites, commonly encountered with ion engines, can be avoided.

While electrostatic charge has not been applied so far to perform relative motion control, the possibility of active charge control in a craft has been demonstrated by several missions like SCATHA[2] and ATS missions.[3] A more recent example is the CLUSTER mission[4,5,6] consisting of 4 craft, where an active charge control is used to nullify the relative potential between the spacecraft and plasma environment.

*Graduate Student, Virginia Tech, Blacksburg VA 24060.

†Associate Professor, H. Joseph Smead Fellow, University of Colarado, Boulder CO 80309.

A simplified case of Coulomb formation flying is a Coulomb tether formation, which consists of 2 spacecraft capable of controlling their electrostatic charge. In such a formation, a line-of-sight electrostatic force replaces a conventional physical tether. The resulting equations of motion are very similar to a regular 2-craft physical tether system with the following differences. The Coulomb tether is capable of producing both attractive and repulsive forces, compared to the tension only forces of the physical tether. Further, the latter can introduce additional complicated flexing dynamics, while the former allows for the equivalent tether stiffness to be tuned through feedback gains. While a regular physical tether mission typically envisions kilometer size tethers, the Coulomb tether concept is only practical for relatively short separation distances ranging up to 100 meters. Sample applications include the deployment of a small sensor from a mother craft to provide an external monitor, or performing controlled proximity and docking approach maneuvers.

The concept of formation flying using electrostatic propulsion is introduced in References 1, 7 and 8. These pioneering works discussed the static Coulomb satellite formations and the associated equilibrium charges, but did not address the active stabilization of these formations. The NIAC (NASA Institute for Advanced Concepts) report by King et al.[1] develops analytical solutions for Hill-frame invariant Coulomb formations. Here spacecraft are placed at specific locations in the rotating Hill frame with constant electrostatic charges. As a result, the Coulomb forces perfectly cancel all Keplerian relative orbit accelerations, thus causing the satellites to remain fixed or static as seen by the constantly rotating Hill frame. The analytical solutions were found for simple geometries involving 3 to 7 satellites using formation symmetry. In all these formations one satellite is located at the center of mass of the satellite formation. The equations of motion representing these Coulomb formations in the Hill frame are highly coupled, non-linear equations. With multiple craft, complex static formations other than the simple symmetric formations found in Reference 8, are also possible. However, these complex static formations are non-intuitive and a numerical approach is often needed to find the constant Hill frame position and charge that result in a static formation. One such numerical approach using a genetic algorithm is given in Reference 9. In Reference 9, Coulomb formation shapes involving up to 9 craft are discussed. The necessary conditions for achieving such static Coulomb formations are determined in Reference 10 using a Hamiltonian formulation of the Coulomb formation dynamics. These Hamiltonian formulations are analogous to the study of equilibrium conditions of rigid bodies in orbit. The analytical solution for the static charge and their feasibility for different shapes in two-craft and three-craft formations are discussed in detail in Reference 11. Romanelli et al.[12] showed that Coulomb forces can be used to cancel the differential drag due to solar radiation, J_2 effects and atmospheric drag, experienced by craft in a static formation. Note that the charge is held constant in the above mentioned open-loop static Coulomb formations studies. All these open-loop static Coulomb formations are found to be unstable without feedback.

Reference 7 discusses static Coulomb satellite formations and a nonlinear control law which is capable of bounding the relative motion between two close craft by controlling the semi-major axis difference. This charge feedback control can also be used to control general orbit element differences with guaranteed stability, but not necessarily with asymptotic convergence. Reference 13 presents an open loop stable spinning two craft Coulomb tether. The reconfiguration of this spinning Coulomb tether in deep space is also discussed, but orbital motion is not considered. A Lyapunov-based control law for stabilizing a 1D-restricted three-craft Coulomb structure is shown in Reference 14. The Lyapunov-based control law identifies the required charge products. Real implementable charge values for each craft are extracted by studying the null space of the charge product matrix. A control law for avoiding collision between spacecraft in a cluster in free space is proposed in Reference 15. This control law requires only the separation distance between the craft and its rate for determining the charge feedback. The control law ensured

that no two craft were within each other's safety spherical zones of fixed radius.

Studies pertaining to tethered spacecraft formation flying using Coulomb forces include 16, 17 and 18. Reference 16 investigates the regulation of a specific shape and orientation of a static two-craft Coulomb tether formation aligned along the orbit radial direction. Charge feedback control laws for asymptotically stabilizing the formation are developed, leading to the first stable virtual Coulomb structure. Reference 17 studies the reconfiguration of the 2-craft Coulomb tether formation by forcing the craft to move apart or come closer. An active charge feedback law is introduced and the linear stability of the coupled separation distance and attitude is evaluated for this time-variant system. Based on this analysis, stability regions for expanding and contracting the two-craft formation are established. The present work is a continuation of this investigation of the nadir-aligned two-craft Coulomb tether. Two specific aspects in the context of reconfiguration are dealt with. One pertains to variation of out-of-plane angle and the other pertains to curtailment of separation distance oscillation. Reference 18 discusses the reconfiguration problem of a Coulomb tether aligned along the orbit-normal and along-track directions. For the orbit-normal configuration the linearized shape dynamics are found to be passively stable, while both in-plane and out-of-plane orientations decoupled from the charge control and were unstable. The along-track configuration has the out-of-plane motion decoupled similar to the orbit-nadir aligned case, and requires a hybrid Coulomb and conventional thrusting control strategy to stabilize the shape.

The present paper focuses solely on the charged relative motion for the orbit nadir aligned configuration. Analytical solutions to the out-of-plane motion are explored for cases of constant rate of change in the length of the Coulomb tether. This, for example, is a typical scenario where a sensor is desired to be deployed to a specified distance, and the reference separation distance is varied at a fixed rate. The analytical solutions are compared with the actual nonlinear response using numeric simulations. Considering the emphasis of the paper on the utility of the analytical solution, the measurement errors and white noises are being ignored in the numerical simulation. Adding them would make the comparison difficult to interpret.

Employing a fixed separation rate maneuver requires infinite acceleration at the beginning and end of the maneuver due to the impulsive change in the desired separation rate. In Reference 17 this causes noticeable transient tracking errors at the maneuver end points. The feedback control is able to stabilize these. However, this paper investigates, in addition, smoothed reference separation rate strategies with the goal of reducing the resulting tracking error transients.

This paper is organized as follows. First, the analytical solution for the linearized out-of-plane angle equation of motion (EOM) is derived and this is followed by establishing the bounds on the initial out-of-plane angle. Next a smooth transition function is defined, followed by adapting this function for the reference length rate problem. Finally, numerical simulations illustrate the results.

Problem Statement

The notation and variables of References 16 and 17 are used in this study. The basic Coulomb tether structure used is shown in Figure 1. The separation distance L between the craft is written as

$$L = L_{\text{ref}} + \delta L \tag{1}$$

where L_{ref} is the ideal reference length and δL is the small deviation (error) from it. Note, the reference length L_{ref} may be constant (as in regulation problem) or varying with time (as in reconfiguration problem). Assuming small angular deviations of ψ and θ, the linearized equations of motion describing the dynamics of two-craft Coulomb

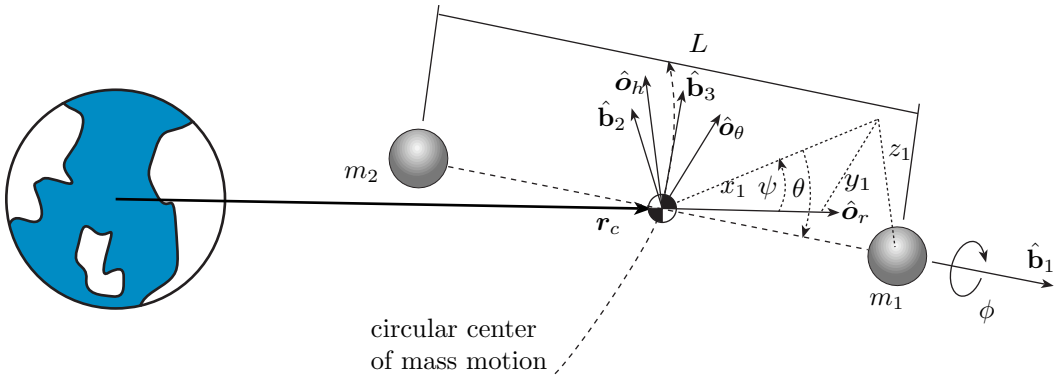

Figure 1. Coulomb tethered two satellite formation with the satellites aligned along the orbit nadir direction

tether reconfiguration are:[17]

$$\ddot{\theta} + \frac{2\dot{L}_{\text{ref}}}{L_{\text{ref}}}\dot{\theta} + 4\Omega^2\theta = 0 \tag{2a}$$

$$\ddot{\psi} + \frac{2\dot{L}_{\text{ref}}}{L_{\text{ref}}}\dot{\psi} + \frac{2\Omega}{L_{\text{ref}}}\delta\dot{L} - \frac{2\dot{L}_{\text{ref}}}{L_{\text{ref}}^2}\Omega\delta L + \frac{2\dot{L}_{\text{ref}}}{L_{\text{ref}}}\Omega + 3\Omega^2\psi = 0 \tag{2b}$$

$$\delta\ddot{L} + \ddot{L}_{\text{ref}} - 2\Omega L_{\text{ref}}\dot{\psi} - 9\Omega^2\delta L - \frac{k_c}{m_1}\delta Q\frac{1}{L_{\text{ref}}^2}\frac{m_1+m_2}{m_2} = 0 \tag{2c}$$

where the in-plane angle ψ and the out-of-plane angle θ describe the attitude of the formation, δL is the error in the separation distance between the two crafts. The constant chief orbital rate is given by $\Omega = \sqrt{\mu/r_c^3}$, where μ is the gravitational coefficient and $\boldsymbol{r}_c$ is center of mass position vector. The parameter $k_c = 8.99 \cdot 10^9$ Nm^2/C^2 is the Coulomb constant. Let q_i be the individual spacecraft charges, then $Q = q_1 q_2$ is the charge product of the 2 craft. The prescribed reference length and its rate are given by L_{ref} and $\dot{L}_{\text{ref}}$. Finally, the constants m_1 and m_2 are the masses of the two craft. The feedback control law is introduced through the charge product variation term δQ and is written as

$$\delta Q = \frac{m_1 m_2 L_{\text{ref}}^2(t)}{(m_1+m_2)\,k_c}(-C_1\delta L - C_2\delta\dot{L}) \tag{3}$$

where C_1 and C_2 are the position and velocity gains and the actual commanded charge product is:

$$Q = Q_{\text{ref}} + \delta Q \tag{4}$$

The reference charge product for a nadir aligned 2 charged craft equilibrium is[11,16]

$$Q_{\text{ref}} = -3\Omega^2\frac{L_{\text{ref}}^3}{k_c}\frac{m_1 m_2}{m_1+m_2} \tag{5}$$

The linearized closed-loop equations in Eqs. (2) are the result of this charge feedback control law. These EOM reveal that the out-of-plane angle (θ) is decoupled from the in-plane angle (ψ) and the separation distance error (δL). Hence, the out-of-plane angle can not be actively controlled by the Coulomb force. For the regulation problem the out-of-plane angle EOM is a time-invariant second order differential equation that results in a stable simple harmonic oscillation motion for θ. Whereas, for the reconfiguration problem the EOM is a second order differential equation with time dependent terms that involve the prescribed reference length (L_{ref}) and reference length rate ($\dot{L}_{\text{ref}}$). Depending on whether one is expanding (positive $\dot{L}_{\text{ref}}$) or contracting (negative $\dot{L}_{\text{ref}}$) the Coulomb tether formation, the initial out-of-plane angle oscillations will decrease or increase respectively. The contracting operation is of particular interest in that it has potential applications in space structure docking operations. These docking operations might require the final angular oscillations to be within prescribed limits to satisfy mechanical mating tolerances. The in-plane angle can be asymptotically controlled by using the Coulomb force. This now leaves the out-of-plane angle and we are interested in developing certain bounds on the initial out-of-plane oscillation such that the finial oscillation is within the prescribed limits. This paper investigates analytical solutions for the out-of-plane angle EOM when the reference length rate ($\dot{L}_{\text{ref}}$) is a constant. For the reconfiguration problem, the user is free to prescribe an appropriate rate of change for the reference length ($\dot{L}_{\text{ref}}$) within the stable regions discussed in Reference 17.

Analytical Solution for Out-of-Plane Motion

The linearized equation of motion for the charged spacecraft out-of-plane angular motion is given in Eq. (2a) as

$$\ddot{\theta} + 2\frac{\dot{L}_{\text{ref}}}{L_{\text{ref}}}\dot{\theta} + 4\Omega^2\theta = 0 \tag{6}$$

Note that the spacecraft charges q_i do not enter this linearized equation. Only with large out-of-plane motion does the spacecraft charge begin to have an influence. For a constant reference length rate ($\dot{L}_{\text{ref}}$), the reference length is written as

$$L_{\text{ref}}(t) = L_0 + \dot{L}_{\text{ref}}\, t \tag{7}$$

where L_0 is the initial reference separation distance and t is the time. Substituting Eq. (7) back into the out-of-plane equation of motion given in Eq. (6) results in

$$\ddot{\theta} + 2\frac{\dot{L}_{\text{ref}}}{L_0 + \dot{L}_{\text{ref}}\, t}\dot{\theta} + 4\Omega^2\theta = 0 \tag{8}$$

An analytical solution for the equation of motion given in Eq. (8) is obtained by transforming the equation to the Bessel equation.[19] The detailed derivation of the analytical solution using Bessel functions is presented in the appendix. The analytical solution to the out-of-plane differential equation in (6) is given by

$$\theta(t) = \frac{1}{L_0 + \dot{L}_{\text{ref}}\, t}\left(A\sin\left(\frac{2\Omega L_0}{\dot{L}_{\text{ref}}} + 2\Omega t\right) + B\cos\left(\frac{2\Omega L_0}{\dot{L}_{\text{ref}}} + 2\Omega t\right)\right) \tag{9}$$

The arbitrary constants A and B can be evaluated using the initial conditions. Let the initial conditions (i.e. at $t = 0$) of out-of-plane angle (θ) and its rate ($\dot{\theta}$) be

$$\theta(0) = \theta_0 \tag{10}$$

$$\dot{\theta}(0) = \dot{\theta}_0 \tag{11}$$

From Eq. (9), the expression for θ at $t = 0$ can be written as

$$\theta(0) = \frac{1}{L_0}\left(A\sin\left(\frac{2\Omega L_0}{\dot{L}_{\text{ref}}}\right) + B\cos\left(\frac{2\Omega L_0}{\dot{L}_{\text{ref}}}\right)\right) \tag{12}$$

Comparing Eq. (10) and Eq. (12) leads to

$$A\sin\left(\frac{2\Omega L_0}{\dot{L}_{\text{ref}}}\right) + B\cos\left(\frac{2\Omega L_0}{\dot{L}_{\text{ref}}}\right) = L_0\theta_0 \tag{13}$$

Taking the time derivative of Eq. (9), the expression for angle rate ($\dot{\theta}$) is written as

$$\begin{aligned}\dot{\theta}(t) &= \frac{-\dot{L}_{\text{ref}}}{(L_0 + \dot{L}_{\text{ref}}\, t)^2}\left[A\sin\left(\frac{2\Omega L_0}{\dot{L}_{\text{ref}}} + 2\Omega t\right) + B\cos\left(\frac{2\Omega L_0}{\dot{L}_{\text{ref}}} + 2\Omega t\right)\right] \\ &\quad + \frac{2\Omega}{L_0 + \dot{L}_{\text{ref}}\, t}\left[A\cos\left(\frac{2\Omega L_0}{\dot{L}_{\text{ref}}} + 2\Omega t\right) - B\sin\left(\frac{2\Omega L_0}{\dot{L}_{\text{ref}}} + 2\Omega t\right)\right]\end{aligned} \tag{14}$$

The expression for $\dot{\theta}(t)$ at $t = 0$ is derived from Eq. (14) as

$$\dot{\theta}(0) = \frac{-\dot{L}_{\text{ref}}}{L_0^2}\left[A\sin\left(\frac{2\Omega L_0}{\dot{L}_{\text{ref}}}\right) + B\cos\left(\frac{2\Omega L_0}{\dot{L}_{\text{ref}}}\right)\right] + \frac{2\Omega}{L_0}\left[A\cos\left(\frac{2\Omega L_0}{\dot{L}_{\text{ref}}}\right) - B\sin\left(\frac{2\Omega L_0}{\dot{L}_{\text{ref}}}\right)\right] \tag{15}$$

Again, by comparing Eq. (15) and the initial condition given in Eq. (11), we find

$$A\left[\frac{-\dot{L}_{\text{ref}}}{L_0^2}\sin\left(\frac{2\Omega L_0}{\dot{L}_{\text{ref}}}\right) + \frac{2\Omega}{L_0}\cos\left(\frac{2\Omega L_0}{\dot{L}_{\text{ref}}}\right)\right] + B\left[\frac{-\dot{L}_{\text{ref}}}{L_0^2}\cos\left(\frac{2\Omega L_0}{\dot{L}_{\text{ref}}}\right) - \frac{2\Omega}{L_0}\sin\left(\frac{2\Omega L_0}{\dot{L}_{\text{ref}}}\right)\right] = \dot{\theta}_0 \tag{16}$$

Solving equations Eq. (13) and Eq. (16) for A and B yields

$$\begin{bmatrix} A \\ B \end{bmatrix} = \begin{bmatrix} \sin\left(\frac{2\Omega L_0}{\dot{L}_{\text{ref}}}\right) & \cos\left(\frac{2\Omega L_0}{\dot{L}_{\text{ref}}}\right) \\ \frac{-\dot{L}_{\text{ref}}}{L_0^2}\sin\left(\frac{2\Omega L_0}{\dot{L}_{\text{ref}}}\right) + \frac{2\Omega}{L_0}\cos\left(\frac{2\Omega L_0}{\dot{L}_{\text{ref}}}\right) & \frac{-\dot{L}_{\text{ref}}}{L_0^2}\cos\left(\frac{2\Omega L_0}{\dot{L}_{\text{ref}}}\right) - \frac{2\Omega}{L_0}\sin\left(\frac{2\Omega L_0}{\dot{L}_{\text{ref}}}\right) \end{bmatrix}^{-1} \begin{bmatrix} L_0\theta_0 \\ \dot{\theta}_0 \end{bmatrix} \tag{17}$$

which leads to the following solutions for A and B:

$$A = \left(\frac{\dot{L}_{\text{ref}}\theta_0 + L_0\dot{\theta}_0}{2\Omega}\right)\cos\left(\frac{2\Omega L_0}{\dot{L}_{\text{ref}}}\right) + L_0\theta_0\sin\left(\frac{2\Omega L_0}{\dot{L}_{\text{ref}}}\right) \tag{18}$$

$$B = -\left(\frac{\dot{L}_{\text{ref}}\theta_0 + L_0\dot{\theta}_0}{2\Omega}\right)\sin\left(\frac{2\Omega L_0}{\dot{L}_{\text{ref}}}\right) + L_0\theta_0\cos\left(\frac{2\Omega L_0}{\dot{L}_{\text{ref}}}\right) \tag{19}$$

Thus, Eq. (18) and Eq. (19) give the expressions for the constants of integration A and B.

The analytical solution given in Eq. (9) can be further simplified into a single trigonometric function with a phase angle and amplitude. Recall the trigonometric identity

$$X\sin\theta + Y\cos\theta = \sqrt{X^2 + Y^2}\cos\left(\theta - \tan^{-1}\left(\frac{X}{Y}\right)\right) \tag{20}$$

Now, using this trigonometric identity, the analytical expression for $\theta(t)$ given in Eq. (9) is rewritten as

$$\theta(t) = \frac{1}{L_0 + \dot{L}_{\text{ref}}\, t}\sqrt{A^2 + B^2}\cos\left(\frac{2\Omega L_0}{\dot{L}_{\text{ref}}} + 2\Omega t - \tan^{-1}\left(\frac{A}{B}\right)\right) \tag{21}$$

Therefore, Eq. (21) provides the final form of the analytical solution with constants A and B defined in Eq. (18) and Eq. (19).

Bounds on Initial Out-Of-Plane Angle

This section investigates analytical bounds on how much out-of-plane motion will be present at the end of the Coulomb tether constant expansion or contraction maneuver. With such results it is possible to predict if conventional thrusting must be employed to reduce the current out-of-plane motion before engaging the maneuver. By studying Eq. (21), the time varying amplitude of the out-of-plane angle θ is written as

$$[\theta(t)]_{\text{amp}} = \frac{1}{L_0 + \dot{L}_{\text{ref}}\, t}\sqrt{A^2 + B^2} \tag{22}$$

The amplitude expression in Eq. (22) is further simplified by substituting the expressions for A and B from Eq. (18) and Eq. (19). The simplified amplitude expression in terms of initial out-of-plane angle θ_0 and initial rate $\dot{\theta}_0$ is given by

$$[\theta(t)]_{\text{amp}} = \frac{1}{L_0 + \dot{L}_{\text{ref}}\, t}\left[\left(\frac{\dot{L}_{\text{ref}}\theta_0 + L_0\dot{\theta}_0}{2\Omega}\right)^2 + (L_0\theta_0)^2\right]^{\frac{1}{2}} \tag{23}$$

The analytical solution using Bessel functions and the time-varying amplitude expression holds for both expansion and contraction of the separation distance between the two satellites. Reference 17 discusses that during expansion the out-of-plane oscillations are reduced due to angular momentum conservation. Therefore, regardless of the initial out-of-plane angle at the beginning of the expansion, one is guaranteed to have a smaller out-of-plane oscillation at the end of an expansion operation. The converse is true for contracting the 2-craft Coulomb tether. The initial out-of-plane oscillation will increase as the satellites are brought closer. We are interested in establishing a bound on the initial oscillation such that the final oscillations at the end of the contraction will be with in a prescribed limit. Let the maximum initial out-of-plane oscillation be $\theta_{0_{\text{max}}}$ while the initial angular rate is zero. The amplitude expression in Eq. (23) is then rewritten as

$$[\theta(t)]_{\text{amp}} = \frac{\theta_{0_{\text{max}}}}{L_0 + \dot{L}_{\text{ref}}\, t}\left[\left(\frac{\dot{L}_{\text{ref}}}{2\Omega}\right)^2 + (L_0)^2\right]^{\frac{1}{2}} \tag{24}$$

For the given initial and final separation distances, and the constant rate of change of separation distance ($\dot{L}_{\text{ref}}$), the total time involved for the contraction operation can be determined. Let this time be given by t_{max}. The desired bound on the out-of-plane oscillation amplitude at the end of the time t_{max} is given by $[\theta(t_{\text{max}})]_{\text{amp}}$. Inserting these values in Eq. (24) results in

$$[\theta(t_{\text{max}})]_{\text{amp}} \geqslant \frac{\theta_{0_{\text{max}}}}{L_0 + \dot{L}_{\text{ref}}\, t_{\text{max}}}\left[\left(\frac{\dot{L}_{\text{ref}}}{2\Omega}\right)^2 + (L_0)^2\right]^{\frac{1}{2}} \tag{25}$$

Rearranging Eq. (25) for $\theta_{0_{\max}}$ gives

$$\theta_{0_{\max}} \leqslant [\theta(t_{\max})]_{\text{amp}} \frac{(L_0 + \dot{L}_{\text{ref}}\, t_{\max})}{\sqrt{\left(\frac{\dot{L}_{\text{ref}}}{2\Omega}\right)^2 + (L_0)^2}} \tag{26}$$

The inequality given in Eq. (26) establishes the bounds on the initial out-of-plane angle . Satisfying this inequality leads to a final out-of-plane oscillation that is less than the permissible value of $[\theta(t_{\max})]_{\text{amp}}$. If out-of-plane thrusting is only to be employed if the final out-of-plane motion is larger than a prescribed amount, then Eq. (26) provides a convenient and simple check.

Smoothed Reconfiguration Rates

Reference 17 presents a charge feedback strategy to reconfigure a nadir-aligned 2-craft Coulomb tether. Let us first review this reconfiguration control strategy. Recall that the parameter $Q = q_1 q_2$ is the charge product of the two spacecraft. The charge feedback strategy in Reference 17 is given by

$$Q(t) = Q_{\text{ref}}(t) + \delta Q(t) \tag{27}$$

where the reference charge is computed using the equilibrium charge condition for a constant reference length L_{ref} using:[16, 11]

$$Q_{\text{ref}} = -3\Omega^2 \frac{L_{\text{ref}}^3}{k_c} \frac{m_1 m_2}{m_1 + m_2} \tag{28}$$

and the charge feedback component δQ is determined through

$$\delta Q = \frac{m_1 m_2 L_{\text{ref}}^2(t)}{(m_1 + m_2)\, k_c} (-C_1 \delta L - C_2 \delta \dot{L}) \tag{29}$$

Only the separation distance between the 2 craft needs to be measured for the feedback. This could be accomplished, for example, using a laser range finder or time coded radio signals. To perform a constant rate nadir-aligned Coulomb tether expansion or contraction, the reference length rate $\dot{L}_{\text{ref}}$ is switched instantaneously from 0 to non-zero at time t_0, and back to zero at the end of the reference maneuver. The system cannot produce these required infinite accelerations with finite charges, and thus some transient error motion results which the charge feedback strategy must stabilize. This section investigates how to smooth this on/off transition to minimize transient effect.

The function $F(t)$ jumps smoothly from zero to one at the point $t = t_0$ as illustrated in Figure 2. This function is based on the hyperbolic tangent function $\tanh(x)$. To represent a value jumping up at $t = t_0$, use

$$F(t) = \frac{1}{2} + \frac{1}{2} \tanh\left(\frac{t - t_0}{\sigma}\right) \tag{30}$$

The hyperbolic tangent function used in Eq. (30) is a monotonically increasing with the value approaching -1 as $t \to -\infty$ and approaching $+1$ as $t \to \infty$. Because of the finite precision involved in computing, the value of hyperbolic tangent function will get rounded off to a constant value of $+1$ for all values of t beyond $(t_0 + 16\sigma)$, and to -1 for all values of t below $(t_0 - 16\sigma)$. Thus, the value of the function $F(t)$ goes to 0 and 1 at $t = (t_0 - 16\sigma)$ and $t = (t_0 + 16\sigma)$, respectively. A plot of the function $F(t)$ is shown in Figure 2 illustrating the symmetry about the point $t = t_0$. An examination of the figure also illustrates that the change in the value of the function $F(t)$ essentially occurs while

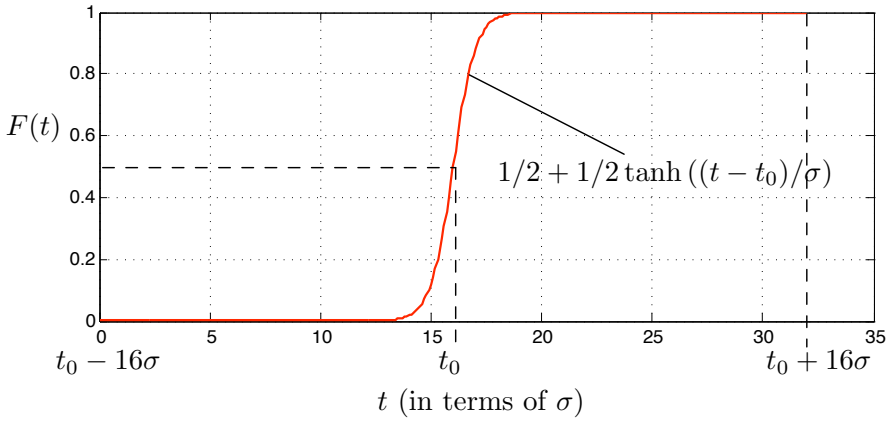

Figure 2. Time history of the smooth transition function $F(t)$.

t lies in a small interval around t_0. The smoothing time interval can be made as small as desired by choosing an appropriate value of σ. Moreover, $t = t_0$ is a point of inflection with the value of the function equal to $1/2$. To smooth the drop to zero commanded rate at the end of the maneuver the function

$$F_e(t) = 1.0 - F(t) \tag{31}$$

can be used.

The function $F(t)$ is infinitely smooth and differentiable to any order. Note that the derivatives of all orders will approach to zero near at $(t_0 \pm 16\sigma)$. This closely matches the ideal characteristics of the constant rate function before and after the jump. The time derivative of function $F(t)$ is obtained using the identity $\text{sech}^2(x) = 1.0 - \tanh^2(x)$, as

$$\dot{F}(t) = \frac{1}{2\sigma}\text{sech}^2\left(\frac{t - t_0}{\sigma}\right) \tag{32}$$

The derivative of $F(t)$ given in Eq. (32) is plotted in Figure 3. It can be seen from the plot that the $\dot{F}(t)$ reaches its maximum value at $t = t_0$.

The commanded length rate $\dot{L}_{\text{ref}}$ around the initial time t_0 is now modified to be

$$\dot{L}_{\text{ref}}(t) = F(t) \cdot \dot{L}_{\text{des}} \tag{33}$$

where $\dot{L}_{\text{des}}$ is the desired constant expansion or contraction rate. The smoothed reference length acceleration at any given point of time is given by

$$\ddot{L}_{\text{ref}}(t) = \frac{\dot{L}_{\text{des}}}{2\sigma}\text{sech}^2\left(\frac{t - t_0}{\sigma}\right) \tag{34}$$

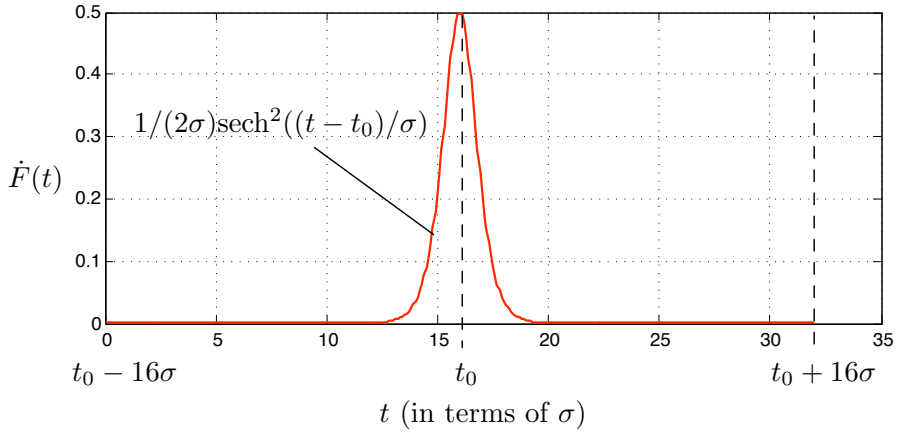

Figure 3. Time history of the time derivative of the smooth transition function ($\dot{F}(t)$).

The maximum acceleration occurs at $t = t_0$ and is written as

$$\ddot{L}_{\text{ref}}(t_0) = \frac{\dot{L}_{\text{des}}}{2\sigma} \tag{35}$$

The change in reference length during this smooth transition is determined by integrating Eq. (33) over the time period $(t_0 - 16\sigma)$ to $(t_0 + 16\sigma)$. The expression for this change in reference length is given as

$$L_{\text{ref}} = \dot{L}_{\text{des}} \left[\frac{1}{2}t + \frac{1}{2} \ln \left(\cosh \left(\frac{t - t_0}{\sigma} \right) \right) \right]_{t_0 - 16\sigma}^{t_0 + 16\sigma} \tag{36}$$

Next, the time period over which this transition should take place must be determined. In other words, the value of σ must be determined. The limiting factor for sigma is the maximum available charge that a spacecraft can safely produce. Consider the nonlinear separation distance equation of motion given below

$$\ddot{L} = (2n\dot{\psi} + 3\Omega^2)L + \frac{k_c}{m_1} Q \frac{1}{L^2} \frac{m_1 + m_2}{m_2} \tag{37}$$

For an ideal equilibrium case, the in-plane angle rate ($\dot{\psi}$) is zero and the separation distance L will track L_{ref}. Implementing this ideal one-dimensionally constrained scenario in Eq. (37) results in

$$\ddot{L}_{\text{ref}} = 3\Omega^2 L_{\text{ref}} + \frac{k_c}{m_1} Q \frac{1}{L_{\text{ref}}^2} \frac{m_1 + m_2}{m_2} \tag{38}$$

Substituting the maximum reference length acceleration from Eq. (35) in to Eq. (38) and

approximating L_{ref} as initial separation length L_0 yields

$$\frac{\dot{L}_{\text{des}}}{2\sigma} = 3\Omega^2 L_0 + \frac{k_c}{m_1} Q \frac{1}{L_0^2} \frac{m_1 + m_2}{m_2} \tag{39}$$

Note, the reference length ($L_{\text{ref}}(t_0)$) at maximum reference acceleration ($t = t_0$) is ideally found by integrating the reference length rate ($\dot{L}_{\text{ref}}$). To avoid the complex integral during the computation of σ, we are using the initial separation distance L_0 with minimal impact on the resulting maximum acceleration prediction. Similarly, while finding the σ needed at the end of the maneuver, the final separation distance (L_f) will be used as an approximation. Let the maximum available charge product be Q_{max}. Using this information in Eq. (39) and rearranging the equation gives the minimum σ required as

$$\sigma_{\text{min}} = \frac{\dot{L}_{\text{des}}}{6\Omega^2 L_0 + 2\frac{k_c}{m_1} Q_{\text{max}} \frac{1}{L_0^2} \frac{m_1+m_2}{m_2}} \tag{40}$$

In all following numerical simulations, we will use at least twice this minimum σ, so that our charge requirement is well with in the limit at any given time.

The reference charge product (Q_{ref}) used in this modified reconfiguration feedback control strategy is also slightly different from the one used in Reference 17. Usually, the reference charge product Q_{ref} is calculated by setting the left hand side of the equation Eq. (38) to zero. That is, the reference length acceleration $\ddot{L}_{\text{ref}}$ is set to zero. Instead the new reconfiguration control strategy incorporates the desired reference separation acceleration into the reference charge product computation. The modified reference charge product is given as

$$Q_{\text{ref}} = \frac{L_{\text{ref}}^2}{k_c} \frac{m_1 m_2}{m_1 + m_2} (\ddot{L}_{\text{ref}} - 3\Omega^2 L_{\text{ref}}) \tag{41}$$

This reference charge product could not be used in Reference 17 because the reference length acceleration ($\ddot{L}_{\text{ref}}$) grows to infinity due to the Heaviside step function. The modified Q_{ref} reduces the amount of tracking errors by feed-forward canceling the $\dot{L}_{\text{ref}}$ term in the closed-loop equations in Eq. (2c). However, the reference charge product in Eq. (41) is computed assuming the ideal scenario where the in-plan angle remains zero. Studying the linearized in plane equations of motion in Eq. (2b) shows that a non-zero $\dot{L}_{\text{ref}}$ will cause ψ to become non-zero. Due to the closed-loop stability we are guaranteed that ψ will remain small and stable. With only line-of sight electrostatic forces it it impossible to perform this reconfiguration maneuver and maintain ψ zero at all time. This would required in-plane lateral thrusting which is not available with Coulomb forces.

Numerical Simulations

In this section, the performance of the smoothed reference length rate transition function and the new reference charge product is illustrated using simulations. This is followed by numeric simulations to illustrate the analytical solution of the out-of-plane motion and to verify the final oscillation predictions.

The Coulomb tether performance with a smoothed reference length rate is simulated in two different manners. First the linearized spherical coordinate differential equations in Eqs. (2) are integrated. This simulation illustrates the expected linear performance of the smoothed reference length rate and the new reference charge product. Second, the linearized results are compared with those obtained from integration of the exact

Table 1. Input parameters used in orbit-radial reconfiguration simulation with smooth transition

Parameter	Value	Units
m_1	150	kg
m_2	150	kg
k_c	8.99×10^9	Nm^2/C^2
Ω	7.2915×10^{-5}	rad/sec
$\delta L(0)$	0.0	m
$\psi(0)$	0.0	rad
$\theta(0)$	0.0	rad
C_1	$12\Omega^2$	
C_2	2.4249Ω	

nonlinear equation of motion of the deputy satellites given by

$$\ddot{\boldsymbol{r}}_1 + \frac{\mu}{r_1^3}\boldsymbol{r}_1 = \frac{k_c}{m_1}\frac{Q}{L^3}(\boldsymbol{r}_1 - \boldsymbol{r}_2) \tag{42a}$$

$$\ddot{\boldsymbol{r}}_2 + \frac{\mu}{r_2^3}\boldsymbol{r}_2 = \frac{k_c}{m_2}\frac{Q}{L^3}(\boldsymbol{r}_2 - \boldsymbol{r}_1) \tag{42b}$$

where $\boldsymbol{r}_1 = \boldsymbol{r}_c + \boldsymbol{\rho}_1$ and $\boldsymbol{r}_2 = \boldsymbol{r}_c + \boldsymbol{\rho}_2$ are the inertial position vectors of the the masses m_1 and m_2, while $L = \sqrt{(\boldsymbol{r}_2 - \boldsymbol{r}_1)\cdot(\boldsymbol{r}_2 - \boldsymbol{r}_1)}$ and μ is the gravitational coefficient. After integrating the motion using inertial Cartesian coordinates, the separation distance L, as well as the in-plane and out-of-plane angles ψ and θ, are computed in post-processing using the exact kinematic transformations.

The first maneuver considered expands the Coulomb tether formation from 25m to 35m in 1.8 days. The simulation parameters used are listed in Table 1. The values of the initial attitude ($\psi(0)$, $\theta(0)$) and the separation length error ($\delta L(0)$), as well as all initial rates, are set to zero. In the reconfiguration simulations in reference 17, the initial tracking errors are due to both initial condition errors and the sudden jumps in reference length (L_{ref}) rate due to the Heaviside function. In order to isolate and show that the oscillations due to the latter have been reduced, the initial conditions are all taken to be zero.

Before running the simulation, the necessary σ values must be computed. Initially, at the start of the reconfiguration the reference length is 25 m and the maximum available charge on each craft is 5 μC. The minimum required σ is calculated using Eq. (40) as

$$\sigma_{1_{\text{min}}} \quad = \quad 6.1905$$

Similarly, the minimum σ value needed at the end of reconfiguration is calculated using the final separation distance of 35 m as $\sigma_{2_{\text{min}}} = 10.70$. The following numerical results use $\sigma_1 = 15$ and $\sigma_2 = 30$ which are more than twice the minimum required to avoid charge saturation. The σ_i values only determine the required maximum required acceleration of the open-loop feed-forward control components. Using this safety factor of 2 helps avoid charge saturation when the shape error feedback control component is added.

Figure 4(a) shows the Coulomb tether motion for increasing the separation distance from 25m to 35m in the linearized spherical coordinates $(\psi, \theta, \delta L)$, along with the spherical coordinates deduced from the full nonlinear equations shown as dotted lines. The

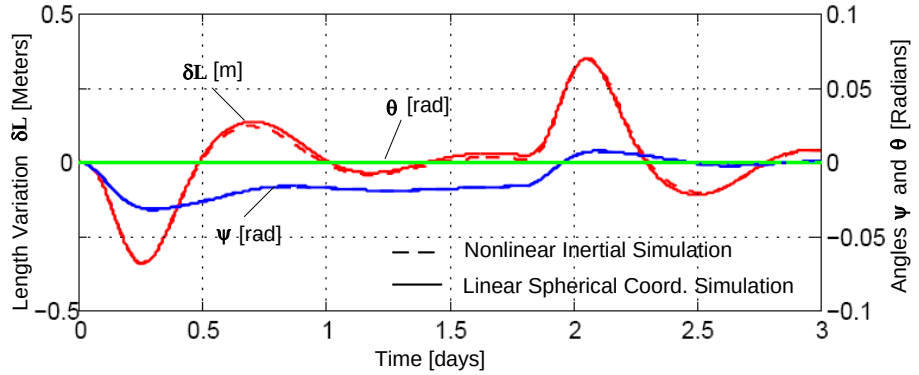

(a) Time histories of length variation δL, in-plane rotation angle ψ, and out-of-plane rotation angle θ for smoothed reference length rate transition.

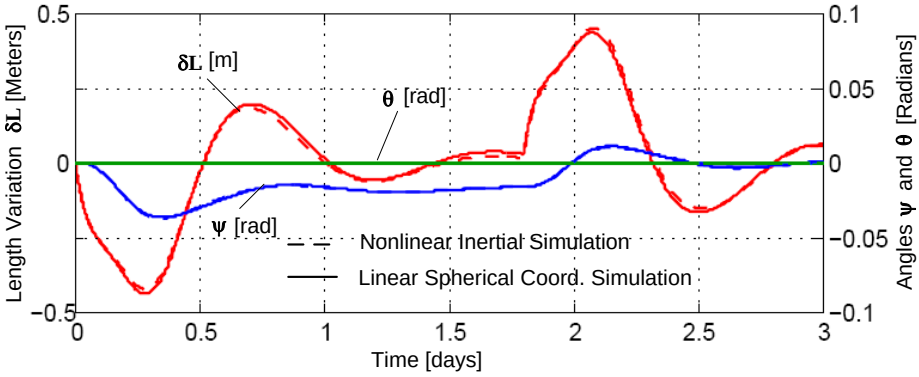

(b) Time histories of length variation δL, in-plane rotation angle ψ, and out-of-plane rotation angle θ for reference length rate transition using Heaviside function.

Figure 4. Coulomb tether states simulation results for expanding the spacecraft separation distance from $25\ m$ to $35\ m$ in 1.8 days. The feedback gains are $\tilde{C}_1 = 12$ and $\tilde{C}_2 = 2.4249$.

expansion is done in 1.8 days. Figure 4(b) also shows the simulation of the same maneuver but, without the smoothed reference length transition function. By comparing the two figures it can be concluded that the oscillations in the in-plane angle (ψ) and separation distance error (δL) are reduced approximately by 10% and 20%, respectively. The in-plane angle is coupled to the separation distance error equation through the in-plane angle rate ($\dot{\psi}$), which is not modeled in to the reference charge. This is the reason for the initial oscillation even though the initial error in the states are zero. The out-of-plane angle (θ) is constantly zero since it is decoupled from the other two states and its initial states are zero to begin with. Figure 5(a) shows the spacecraft control charge q_1 (on craft 1) for both the linearized and full nonlinear simulation models. Both are nearly on top of the reference value pertaining to the static equilibrium at each instant of time. The spikes in control charge observed in the graph are due to the finite reference length accelerations during the smooth reference length rate transition. Note that spikes are well within the 5 μC charge saturation level for this example.

In order to illustrate how well the system is tracking the prescribed reference trajec-

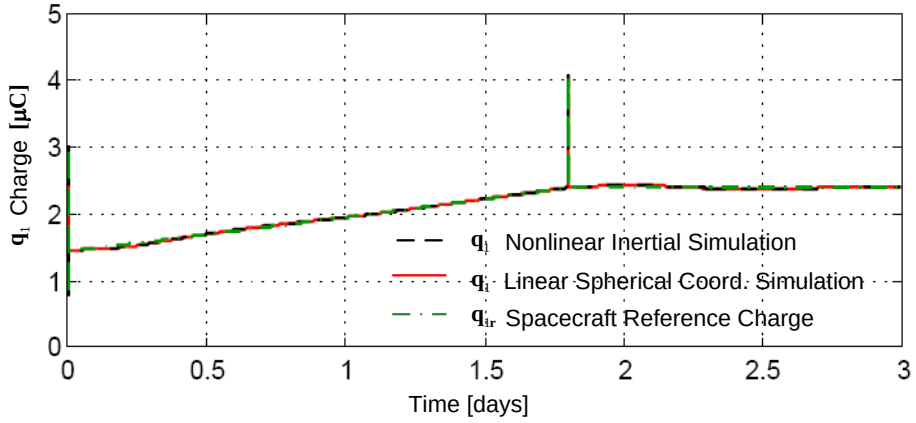

(a) Spacecraft charge time histories for smoothed reference length rate transition.

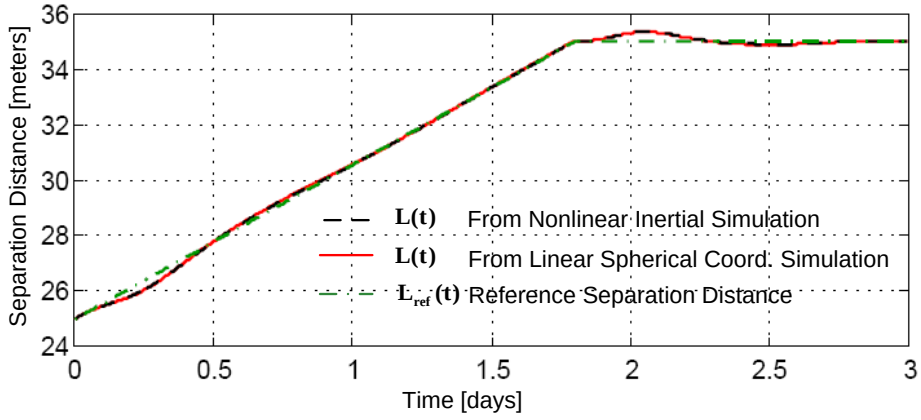

(b) Time histories of separation distance for smoothed reference length rate transition.

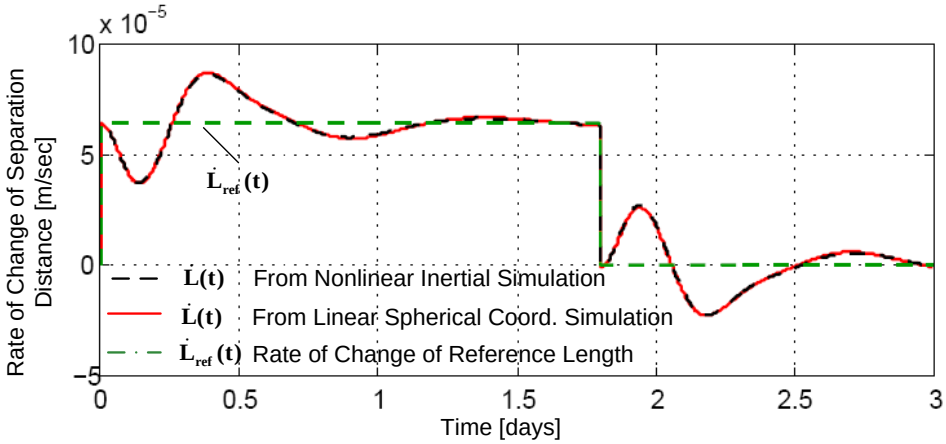

(c) Time histories of rate of change of separation distance for smoothed reference length rate transition.

Figure 5. Charge and tether length simulation results for expanding the spacecraft separation distance from $25\ m$ to $35\ m$ in 1.8 days. The feedback gains are $\tilde{C}_1 = 12$ and $\tilde{C}_2 = 2.4249$.

tory $L_{\text{ref}}(t)$, the time histories of separation distance $L(t)$ and the time histories of rate of change of separation distance $\dot{L}(t)$ are shown in Figure 5(b) and Figure 5(c) , respectively. Figure 5(b) shows that the reference separation distance ($L_{\text{ref}}(t)$) increases linearly until 1.8 days before settling to a constant value and both the linear and inertial nonlinear simulations track the reference separation distance perfectly. Figure 5(c) illustrates that the rate of change of the reference separation distance ($\dot{L}_{\text{ref}}(t)$) is a smoothed representation of a discrete step change.

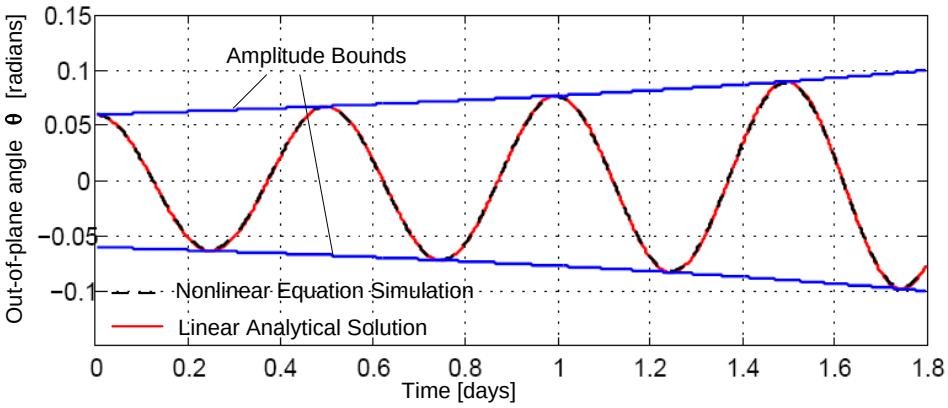

Figure 6. The time histories of the out-of-plane angular motion (θ) using the analytical solution and by simulating the full nonlinear equation. The initial θ value is 0.06 radians, resulting in the final out-of-plane angular oscillation amplitude of 0.1 radians.

Now, in order to verify and illustrate the analytical out-of-plane motion solution, a maneuver is considered involving the contraction of the separation distance between the two satellites from 25 m to 15 m in 1.8 days. When the satellite formation is expanded the amplitude of oscillation decreases due to conservation of momentum. Whereas, while contracting the formation, the amplitude of out-of-plane oscillation increases due to conservation of momentum. This increased out-of-plane oscillation has the potential to make the charge control laws developed based on small angle linearization inaccurate and destabilize the formation. Therefore, it is important to show that the out-of-plane angle oscillation can be kept sufficiently small during contraction maneuver by placing bounds on the initial oscillation. Hence, the choice of contraction maneuver for illustrating the out-of-plane analytical solution.

First, let us calculate the bound on the initial out-of-plane angle (θ) value so that the final oscillation will be not exceed 0.1 rad. Using Eq. (23) and substituting the corresponding values gives

$$\begin{aligned} \theta_{0_{\max}} &\leqslant [\theta(t_{\max})]_{\text{amp}} \frac{(L_0 + \dot{L}_{\text{ref}}\, t_{\max})}{\sqrt{\left(\frac{\dot{L}_{\text{ref}}}{2\Omega}\right)^2 + (L_0)^2}} \\ &\leqslant 0.06 \text{ rad} \end{aligned} \tag{43}$$

Therefore, the maximum initial out-of-plane angle should not exceed 0.06 rad. Assume that while starting the contraction maneuver the out-of-plane angle is at its maximum possible value. This results in setting the initial out-of-plane angle and angle rate as

$\theta = 0.06$ radians and $\dot{\theta} = 0$ rad/sec, respectively. Except for the smoothing function $F(t)$ being turned off, all other parameters and initial values are same as the previous simulation.

The out-of-plane angle equation of motion shown in Eq. (6) is the linearized decoupled equation. As in the previous simulation, we compare its performance with the full nonlinear equation given by Eq. (42). The simulation results are illustrated in Figure 6. The analytical solution in Eq. (9) of the linearized equation for the out-of-plane angle (θ) closely follows the actual out-of-plane angle time history obtained by simulating the full nonlinear equation and error is with in ± 0.0017 radians. The amplitude of the oscillation found using the equation Eq. (23) is shown as the bound and the final out-of-plane angular oscillation amplitude is 0.1 radians as expected.

Recall that the analytical solution for out-of-plane motion and the bound on the initial oscillation is derived assuming that the reference length rate ($\dot{L}_{\text{ref}}$) is a constant. But, in the subsequent section the smooth transition function $(F(t)$ is used at the beginning and end of the maneuver. The effect of this smooth transition function on the out-of-plane angle oscillation prediction is of interest. Consider the same maneuver of expanding the Coulomb tether formation from 25m to 35m in 1.8 days used in the first simulation. Set the initial out-of-plane angle and rate as $\theta = 0.1$ radians and $\dot{\theta} = 0$ rad/sec, respectively. Again, all other parameters and initial values are same as the first simulation. The out-of-plane motion based on the analytical solution (continuous line) and the full nonlinear equation simulation with smoothed reference length rates (dashed line) are shown in Figure 7. There is no appreciable difference in the out-of-plane motion history from the nonlinear simulation and the error is with in ± 0.0024 radians. It still very closely follows the analytical solution results in spite of the smoothed reference length rate.

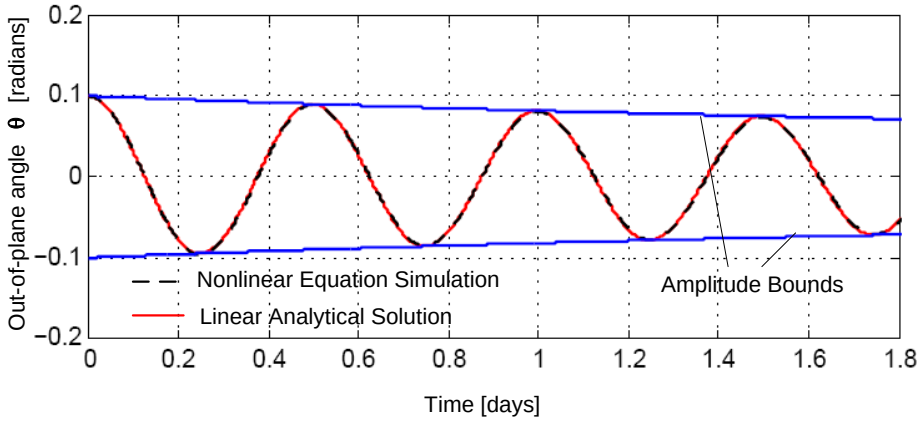

Figure 7. The time histories of the out-of-plane angular motion (θ) using the analytical solution and by simulating the full nonlinear equation with smoothed transition rates.

Conclusion

The analytical solution for the linearized out-of-plane angle (θ) equation of motion for the ideal constant rate reconfiguration problem is developed using the Bessel functions. This solution is used to obtain bounds on the initial out-of-plane angle so that the final out-of-plane angular oscillations is within the prescribed limit. Numerical simulations of the full nonlinear motion are carried out comparing the linearized performance pre-

dictions to the actual nonlinear system response. Further, a smooth transition function is used in the beginning and end of the prescribed constant reference length rate. This eliminates the abrupt increase or decrease of the reference length rate resulting in a finite acceleration at the points of transition. Simulation results show very good tracking with substantially reduced transient error motion. The introduction of this smoothing function has negligible effect on the idealized out-of-plane oscillation during the reconfiguration maneuver considered.

References

[1] L. B. King, G. G. Parker, S. Deshmukh, and J.-H. Chong, "Spacecraft Formation-Flying using Inter-Vehicle Coulomb Forces," tech. rep., NASA/NIAC, January 2002. http://www.niac.usra.edu.

[2] E. G. Mullen, M. S. Gussenhoven, D. A. Hardy, T. A. Aggson, B. G. Ledley, and E. Whipple, "SCATHA Survey of High-Level Spacecraft Charging in Sunlight," *Journal of the Geophysical Sciences*, Vol. 91, Feb. 1986, pp. 1474–1490.

[3] E. C. Whipple and R. C. Olsen, "Importance of differential charging for controlling both natural and induced vehicle potentials on ATS-5 and ATS-6," *Proceedings of the 3rd Spacecraft Charging Technology Conference*, Nov. 12–14 1980, p. 887. NASA Conference Publication 2182.

[4] K. Torkar and et. al., "Spacecraft Potential Control aboard Equator-S as a Test for Cluster-II," *Annales Geophysicae*, Vol. 17, 1999, pp. 1582–1591.

[5] K. Torkar and et. al., "Active Spacecraft Potential Control for Cluster – Implementation and First Results," *Annales Geophysicae*, Vol. 19, 2001, pp. 1289–1302.

[6] C. P. Escoubet, M. Fehringer, and M. Goldstein, "The Cluster Mission," *Annales Geophysicae*, Vol. 19, No. 10/12, 2001, pp. 1197–1200.

[7] H. Schaub, G. G. Parker, and L. B. King, "Challenges and Prospect of Coulomb Formations," *AAS John L. Junkins Astrodynamics Symposium*, College Station, TX, May 23-24 2003. Paper No. AAS-03-278.

[8] L. B. King, G. G. Parker, S. Deshmukh, and J.-H. Chong, "Study of Interspacecraft Coulomb Forces and Implications for Formation Flying," *AIAA Journal of Propulsion and Power*, Vol. 19, May–June 2003, pp. 497–505.

[9] J. Berryman and H. Schaub, "Static Equilibrium Configurations in GEO Coulomb Spacecraft Formations," *AAS/AIAA Space Flight Mechanics Meeting*, Copper Mountain, Colorado, Jan. 2005. Paper No. AAS 05-104.

[10] H. Schaub, C. Hall, and J. Berryman, "Necessary Conditions for Circularly-Restricted Static Coulomb Formations," *AAS Malcolm D. Shuster Astronautics Symposium*, Paper No. AAS 05–472, Buffalo, NY, June. 12–15 2005.

[11] J. Berryman and H. Schaub, "Analytical Charge Analysis for 2- and 3-Craft Coulomb Formations," *AIAA Journal of Guidance, Control, and Dynamics*, Vol. 30, Nov.–Dec. 2007, pp. 1701–1710.

[12] C. C. Romanelli, A. Natarajan, H. Schaub, G. G. Parker, and L. B. King, "Coulomb Spacecraft Voltage Study Due to Differential Orbital Perturbations," *AAS/AIAA Space Flight Mechanics Meeting*, Tampa, Florida, Jan. 2006. Paper No. AAS 06-123.

[13] H. Schaub and I. I. Hussein, "Stability and Reconfiguration Analysis of a Circulary Spinning 2-Craft Coulomb Tether," *IEEE Aerospace Conference*, Big Sky, MT, March 3–10 2007.

[14] S. Wang and H. Schaub, "One-Dimensional 3-Craft Coulomb Structure Control," *7th International Conference on Dynamics and Control of Systems and Structures in Space*, Greenwich, London, England, July 19–20 2006, pp. 269–278.

[15] S. Wang and H. Schaub, "Spacecraft Collision Avoidance Using Coulomb Forces With Separation Distance Feedback," *AAS Space Flight Mechanics Meeting*, Sedona, AZ, Jan. 28–Feb. 1 2007. Paper AAS 07–112.

[16] A. Natarajan and H. Schaub, "Linear Dynamics and Stability Analysis of a Two-Craft Coulomb Tether Formation," *AIAA Journal of Guidance, Control, and Dynamics*, Vol. 29, Jul.–Aug. 2006, pp. 831–839.

[17] A. Natarajan and H. Schaub, "Reconfiguration of a Nadir-Pointing 2-Craft Coulomb Tether," *Journal of the British Interplanetary Society*, Vol. 60, June 2007, pp. 209–218.

[18] A. Natarajan and H. Schaub, "Hybrid Conrol of Orbit Normal and Along-Track 2-Craft Coulomb Tethers," *AAS/AIAA Space Flight Mechanics Meeting*, Sedona, AZ, Jan. 28–Feb. 1 2007. Paper AAS 07–193.

[19] N. McLachlan, *Bessel Functions for Engineers*. Amen House, London E.C.4: Oxford University Press, second edition ed., 1961.

Appendix

This section translates the out-of-plane equations of motion into the form of a standard form of the Bessel equation. Define a new variable z as follows

$$z = L_0 + \dot{L}_{\text{ref}}\, t \tag{44}$$

$$\frac{\mathrm{d}z}{\mathrm{d}t} = \dot{L}_{\text{ref}} \tag{45}$$

Substituting this new variable z given in Eq. (44) into Eq. (8), and changing the derivatives with respect to t (time) to derivatives with respect to z results in

$$\frac{\mathrm{d}^2\theta}{\mathrm{d}z^2} + \frac{2}{z}\frac{\mathrm{d}\theta}{\mathrm{d}z} + k^2\theta = 0 \tag{46}$$

where $k = \frac{2\Omega}{\dot{L}_{\text{ref}}}$ is a constant parameter of this reconfiguration maneuver. The transformed equation in Eq. (46) is not yet in the standard Bessel equation form and needs one more transformation. Assume, the out-of-plane angle θ to be of the form

$$\theta = z^{-\frac{1}{2}} y(z) \tag{47}$$

Now, the first and second derivative of θ with respect to z can be written as

$$\frac{\mathrm{d}\theta}{\mathrm{d}z} = z^{-\frac{1}{2}}\frac{\mathrm{d}y}{\mathrm{d}z} - \frac{1}{2}yz^{-\frac{3}{2}} \tag{48}$$

$$\frac{\mathrm{d}^2\theta}{\mathrm{d}z^2} = z^{-\frac{1}{2}}\frac{\mathrm{d}^2y}{\mathrm{d}z^2} - z^{-\frac{3}{2}}\frac{\mathrm{d}y}{\mathrm{d}z} + \frac{3}{4}yz^{-\frac{5}{2}} \tag{49}$$

Using Eq. (47), Eq. (48) and Eq. (49), the θ equation of motion given in Eq. (46) can be transformed as

$$\frac{\mathrm{d}^2y}{\mathrm{d}z^2} + \frac{1}{z}\frac{\mathrm{d}y}{\mathrm{d}z} + \left(k^2 - \frac{(1/2)^2}{z^2}\right)y = 0 \tag{50}$$

The standard form of the Bessel equation given in Reference 19 is as follows

$$\frac{\mathrm{d}^2y}{\mathrm{d}z^2} + \frac{1}{z}\frac{\mathrm{d}y}{\mathrm{d}z} + \left(k^2 - \frac{v^2}{z^2}\right)y = 0 \tag{51}$$

and the complete solution for Eq. (51) when v is non-integral, is given by

$$y = AJ_v(kz) + BJ_{-v}(kz) \tag{52}$$

where A and B are constants whose values can be determined using initial conditions.

The Bessel functions $J_v(kz)$ and $J_{-v}(kz)$ are given by

$$J_v = \sum_{r=0}^{\infty} \left((-1)^r \frac{\left(\frac{1}{2}kz\right)^{v+2r}}{r!\Gamma(v+r+1)} \right) \tag{53}$$

$$J_{-v} = \sum_{r=0}^{\infty} \left((-1)^r \frac{\left(\frac{1}{2}kz\right)^{-v+2r}}{r!\Gamma(-v+r+1)} \right) \tag{54}$$

where $\Gamma(*)$ is the Gamma function defined as

$$\Gamma(z) = \int_0^{\infty} e^{-t} t^{z-1} \mathrm{d}t \tag{55}$$

By comparing the equation of motion (EOM) given in Eq. (50) and the standard Bessel equation given in Eq. (51), the analytical solution for the EOM can be written as

$$y = AJ_{1/2}(kz) + BJ_{-1/2}(kz) \tag{56}$$

The Bessel function $J_{1/2}(kz)$ can be written using Eq. (53) as

$$J_{1/2}(kz) = \frac{\left(\frac{1}{2}kz\right)^{1/2}}{\Gamma(3/2)} \left\{ 1 - \frac{(kz)^2}{2.3} + \frac{(kz)^4}{2.3.4.5} - \cdots \right\} \tag{57}$$

The value of the function $\Gamma(3/2)$ is calculated to be $\frac{1}{2}\pi^{\frac{1}{2}}$. Using this value and rearranging Eq. (57), one arrives at

$$J_{1/2}(kz) = \left(\frac{2}{\pi kz}\right)^{1/2} \left\{ kz - \frac{(kz)^3}{2.3} + \frac{(kz)^5}{2.3.4.5} - \cdots \right\}$$

$$J_{1/2}(kz) = \left(\frac{2}{\pi kz}\right)^{1/2} \sin(kz) \tag{58}$$

Similarly, the expression for the $J_{-1/2}(kz)$ boils down to

$$J_{-1/2}(kz) = \left(\frac{2}{\pi kz}\right)^{1/2} \cos(kz) \tag{59}$$

The analytical solution for the out-of-plane angular motion θ can be written by combining Eq. (47), Eq. (56), Eq. (58) and Eq. (59) as

$$\theta = z^{-\frac{1}{2}} \left(A \left(\frac{2}{\pi kz}\right)^{1/2} \sin(kz) + B \left(\frac{2}{\pi kz}\right)^{1/2} \cos(kz) \right) \tag{60}$$

Substituting back the definitions of z and k in Eq. (60), one arrives at the expression for θ as a function of time t, which is written as

$$\theta(t) = \left(\frac{\dot{L}_{\text{ref}}}{\pi\Omega}\right)^{1/2} \frac{1}{L_0 + \dot{L}_{\text{ref}}\, t} \left(A \sin\left(\frac{2\Omega L_0}{\dot{L}_{\text{ref}}} + 2\Omega t\right) + B \cos\left(\frac{2\Omega L_0}{\dot{L}_{\text{ref}}} + 2\Omega t\right) \right) \tag{61}$$

The term $\left(\frac{\dot{L}_{\text{ref}}}{\pi\Omega}\right)^{1/2}$ is a constant and can be absorbed in to the arbitrary constants A and B. Therefore, Eq. (61) can be rewritten as

$$\theta(t) = \frac{1}{L_0 + \dot{L}_{\text{ref}}\, t}\left(A\sin\left(\frac{2\Omega L_0}{\dot{L}_{\text{ref}}} + 2\Omega t\right) + B\cos\left(\frac{2\Omega L_0}{\dot{L}_{\text{ref}}} + 2\Omega t\right)\right) \tag{62}$$